

Deterministic Image-to-Image Translation via Denoising Brownian Bridge Models with Dual Approximators

Bohan Xiao^{1*}, Peiyong Wang^{2*}, Qisheng He¹, Ming Dong¹

Department of Computer Science, Wayne State University¹, Detroit, Michigan, USA

Department of Mathematics, Wayne State University², Detroit, Michigan, USA

{gk6511, pywang, qisheng.he, mdong}@wayne.edu

Abstract

Image-to-Image (I2I) translation involves converting an image from one domain to another. Deterministic I2I translation, such as in image super-resolution, extends this concept by guaranteeing that each input generates a consistent and predictable output, closely matching the ground truth (GT) with high fidelity. In this paper, we propose a denoising Brownian bridge model with dual approximators (Dual-approx Bridge), a novel generative model that exploits the Brownian bridge dynamics and two neural network-based approximators (one for forward and one for reverse process) to produce faithful output with negligible variance and high image quality in I2I translations. Our extensive experiments on benchmark datasets including image generation and super-resolution demonstrate the consistent and superior performance of Dual-approx Bridge in terms of image quality and faithfulness to GT when compared to both stochastic and deterministic baselines. Project page and code: <https://github.com/bohan95/dual-app-bridge>

1. Introduction

Image-to-Image (I2I) translation is a significant area of research with broad applications across academia and industry. It involves transforming an image from one domain to another while preserving essential features. Key tasks in this field include generating realistic images from semantic labels [24, 40, 42, 57], transforming segmentation masks into photo-like outputs [40, 47, 54], and enhancing image quality through super-resolution [8, 28, 52].

Among the wide range of applications, some I2I tasks particularly benefit from deterministic models. For instance, in super-resolution, the goal is to translate a low-resolution image into a high-resolution one while accurately preserving fine details. This task, as shown in recent studies [13, 14], requires consistency and high faithfulness to

ground true (GT) because for a given low-resolution image, there is typically one “correct” high-resolution output that should be produced. In such an I2I task, we note that *faithfulness or fidelity is to the individual GT*, not just to the distribution of GT. Any variability in the generated output could result in artifacts or loss of critical information, making stochastic approaches less desirable. Similarly, in tasks such as denoising [6, 51] or inpainting [4, 39], where missing or noisy parts of an image need to be restored, a deterministic approach is preferred.

Generative Adversarial Networks (GANs) [16] have been instrumental in advancing I2I translation, with models like Pix2Pix [24] and CycleGAN[57] demonstrating impressive results. GANs are deterministic during inference, producing the same output for a given input, which is advantageous for tasks requiring faithfulness. However, GANs often struggle to generate high-quality images, frequently resulting in blurriness and artifacts [1, 21].

Diffusion models, such as Denoising Diffusion Probabilistic Models (DDPM) [19] and Latent Diffusion Models (LDM) [40], generate high-quality images by progressively adding noise to images and learning the reverse process. Bridge models, such as Brownian bridge diffusion models [27, 47], utilize Stochastic Differential Equations (SDEs) to directly interpolate between input and output distributions, allowing precise control over transformations [40, 42]. This approach improves analytical tractability, making bridge models well suited for I2I translations. However, the inherent stochasticity in these models (see Figure 1(a)) complicates tasks where faithful results are required (e.g., image super-resolution and image reconstruction). Unlike traditional diffusion models [19, 40, 43], which start from noise and gradually denoise the input to generate an output, bridge models start from structured data and interpolate between input and output distributions. This difference means that deterministic methods like Probability Flow Ordinary Differential Equations (PF-ODEs) [43], when applied to bridge models, can lead to blurry images [43, 54], resulting in degraded model performance (see Figure 1(b)).

*Both authors contributed equally to this research.

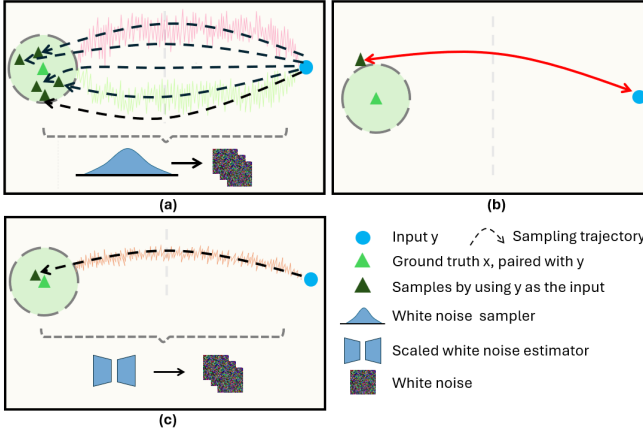


Figure 1. Sampling comparison between SDE-based sampler, PF-ODE-based sampler, and Dual-approx Bridge. The circular area within the dashed circle indicates where the SDE-based sampling outputs land. (a) SDE-based Sampling: diverse outputs of high image quality. (b) PF-ODE-based Sampling: deterministic outputs lack of fine details of ground truth (GT). (c) Dual-approx Bridge Sampling: deterministic output with fine details of GT.

Therefore, there is a growing need for deterministic models that can preserve both image quality and faithfulness in I2I translations.

To resolve this dilemma in the pursuit of deterministic sampling with both high image quality and fidelity, in this paper we propose a denoising Brownian bridge model with Dual Approximators (abbreviated as “Dual-approx Bridge”), a generative model that exploits the Brownian bridge structure to produce faithful output with negligible variance and with an image quality better than or comparable to that generated by SDE-based samplers. More specifically, in the SDE-based structure of a Brownian bridge with both forward and corresponding reverse Brownian motions, we train a neural network in the forward diffusive process to estimate the score function and the initial state in the diffusive iteration. Meanwhile, in the reverse process of the Brownian bridge, a second neural network is trained to approximate the white noise scaled to the time step increment. Here, we emphasize that in deterministic I2I, our goal is to *generate a unique output from a given input, rather than translating probability distributions*, as shown in Figure 1(c). The major contributions of this work are as follows:

- To our best knowledge, Dual-approx Bridge is the first generative model that exploits the Brownian bridge structure to produce faithful output with negligible variance and high image quality for deterministic I2I translations. This is achieved through a novel design of a pair of approximators, trained in the forward and reverse diffusive processes, respectively.
- In Dual-approx Bridge, the reverse approximator optimizes the reverse denoising process and presents an opti-

mal deterministic route for the generative process. From a theoretical perspective, we analyze our model in a general setting where the white noise may take any time-dependent variance.

- Through extensive experiments on benchmark datasets including image generation and super-resolution, we demonstrate the consistent and superior performance of Dual-approx Bridge on image quality and faithfulness to GT when compared to state-of-the-art (SOTA) GAN-based and diffusion-based I2I models.

2. Related Work

In this section, we briefly review the related literature, including image-to-image translation, GAN Models, Diffusion Models, and Bridge Models.

2.1. Image-to-Image Translation

Image-to-image (I2I) translation has become a core task in computer vision [1, 21, 36], focused on learning mappings between the source and target image domains for applications such as style transfer [15] and colorization [9]. Traditional methods, including Pix2Pix [24] and CycleGAN[57], utilize GAN-based architectures to translate images and support diverse I2I tasks by capturing domain-specific features, though challenges remain in maintaining high quality across complex domains [5, 41]. Deterministic I2I translation builds on this by ensuring that each input produces a consistent, predictable output — an essential requirement in fields like medical imaging [29], where precision and reproducibility are crucial. In tasks such as super-resolution [12] or denoising [46], deterministic models can enhance image resolution and clarity without introducing variations that could adversely affect analysis or interpretation.

2.2. Brown Bridge

The Brownian Bridge (BB) [27, 47] is a fundamental stochastic process that models a constrained Brownian motion, where the trajectory is conditioned on fixed start and end points. Unlike an unconstrained Wiener process, which evolves freely, a Brownian bridge interpolates between two known states while maintaining stochastic variations. This property makes it particularly useful in probabilistic modeling, including image-to-image (I2I) translation, conditional generative modeling, and stochastic optimal transport.

2.3. Generative Adversarial Networks

GANs [16] have been pivotal in advancing I2I translation by learning mappings between image domains through adversarial training. One foundational model, Pix2Pix [24], introduced a conditional GAN approach for paired I2I tasks, enabling applications like colorization[7] and semantic label-to-photo translation[24]. For unpaired I2I tasks, CycleGAN [57] employs cycle consistency, allowing the

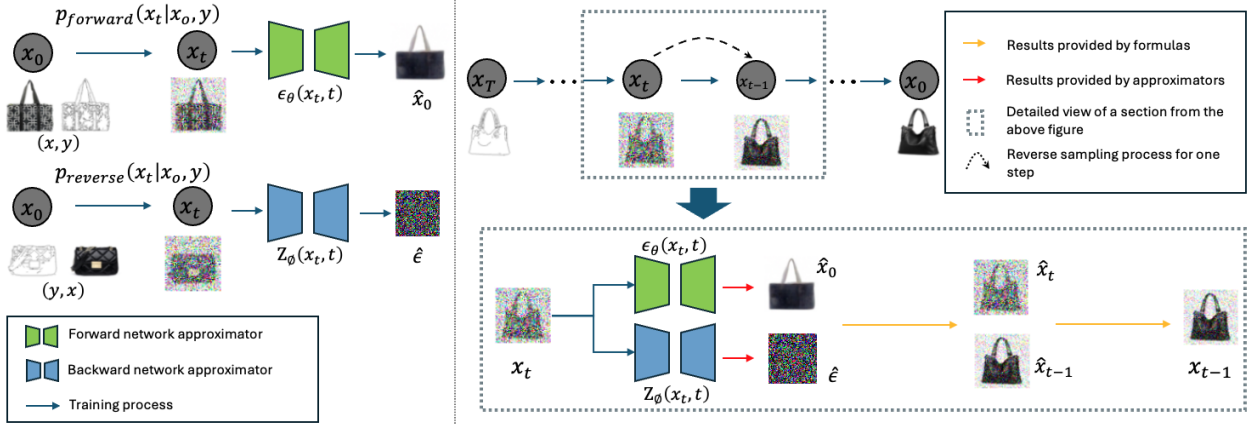


Figure 2. Training process of the two approximators (top-left: forward diffusive process, bottom-left: reverse diffusive process). Right: Sampling workflow with both approximators in action.

model to translate images across domains without requiring paired samples. However, GANs often face artifacts in generated images [5, 41, 50]. Such limitations in image quality, combined with the common challenges of training instability, make GANs less suitable for applications demanding both quality and faithfulness.

2.4. Diffusion and Bridge Models

Diffusion models have established themselves as a leading approach in generative modeling [11] due to their ability to produce high-quality, realistic images through a gradual denoising process. DDPM [20] pioneered this approach, modeling image generation as a series of iterative steps in which random noise is gradually refined into a structured target image. The process results in exceptionally high-quality images with reduced artifacts, often surpassing GANs. LDMs [40] further refined DDPM by focusing on a latent space rather than a pixel space, making the generation process more efficient.

To model the denoising process, diffusion models can rely on two distinct mathematical frameworks: SDEs and PF-ODEs [43]. SDEs, characterized by their inherent randomness, allow the model to generate diverse outputs by gradually reversing noise, enhancing detail and realism, but lacking consistency. This randomness can lead to the same input producing varying outputs. PF-ODEs, on the other hand, remove this randomness, providing a deterministic pathway that produces consistent outputs at the expense of fine details and image richness [27, 43]. Balancing the high image quality provided by SDEs with the consistency achieved by PF-ODEs remains a core challenge in diffusion models.

Bridge models [25, 30, 54] integrate principles from both diffusion and bridge frameworks to create a probabilistic connection between input and output distributions. Both the Schrödinger and Brownian Bridge frameworks [47, 54] have demonstrated significant improvements in im-

age quality across various I2I tasks when compared to traditional diffusion models. However, they inherit certain limitations from both SDE-based and PF-ODE-based sampling. Specifically, they retain the stochastic characteristics of SDEs while also experiencing the lower image quality associated with PF-ODE-based samplers [54].

3. Deterministic Dual-approx Bridge

In this section, we present Dual-approx Bridge in details. The Brownian bridge models [27, 47] have achieved high image quality and diversity in I2I translation. The structure of a Brownian bridge allows it to successfully map between paired probability distributions while generating high quality images of substantial diversity. On the other hand, when it comes to the deterministic I2I translation tasks, diversity is not preferred. In this direction, Dual-approx Bridge delivers deterministic I2I translation with minimal diversity. The key difference between our model and existing diffusion models is that in the generative process, existing models employ one neural network-based approximator which is trained in the forward diffusive process, while we make use of a pair of approximators trained in the forward and reverse diffusive processes separately, shown in Figure 2.

3.1. Score-Based SDE

The score-based Brownian bridge model is prescribed by the forward and reverse SDEs. The forward SDE reads

$$dX = -\frac{X - Y}{1 - t} dt + g(t) dW, \quad t \in (0, 1) \quad (1)$$

where $W(\cdot)$ is a Brownian motion (i.e., a Wiener process), and $g(t)$ is the variance of the white noise. Then $X(1) = Y$.

Let $G(t) = (1-t)^2 \int_0^t \frac{g^2(s)}{(1-s)^2} ds$. It holds that

$$X_t = (1-t)X_0 + tY + (1-t) \int_0^t \frac{g(s)}{1-s} dW(s) \quad (2)$$

$$\sim \mathcal{N}((1-t)X_0 + tY, G(t) I).$$

That is

$$X_t = (1-t)X_0 + tY + \sqrt{G(t)}\epsilon, \quad \epsilon \sim \mathcal{N}(0, I). \quad (3)$$

The reverse generative SDE [2] is given by

$$dX = - \left(\frac{X - Y}{1-t} + g^2(t) \nabla \log p(X, t) \right) dt + g(t) d\bar{W} \quad (4)$$

where $\bar{W}(\cdot)$ is a reverse time Brownian motion, and the *score function* is given by

$$\nabla \log p(X, t) = - \frac{X - (1-t)X_0 - tY}{G(t)}. \quad (5)$$

Hence, in the reverse transitional formula where Δt is the time increment

$$X_{t-1} = X_t + \left(\frac{X_t - Y}{1-t} + g^2(t) \nabla \log p(X_t, t) \right) \Delta t \quad (6)$$

$$- g(t) (\bar{W}(t) - \bar{W}(t - \Delta t))$$

we need to estimate two quantities, X_0 and $\Delta \bar{W} = \bar{W}(t) - \bar{W}(t - \Delta t) = \sqrt{\Delta t} z$, at each time step. In the SDE model, z is just a random variable of the standard normal distribution. This causes the diversity in the output \hat{X}_0 . To make the sampling deterministic, we use a neural network ϵ_θ to estimate X_0 in the forward diffusion process and a second neural network $Z_\phi(X_t, t)$ to estimate z in the reverse diffusion process. That is, we train a pair of dual approximators ϵ_θ and Z_ϕ . Note that our goal here is to generate a unique output from a given input, rather than translating probability distributions. So, we need two neural networks to approximate two different samples for the forward and reverse steps from the same white noise distribution. A single approximator cannot serve this purpose.

3.2. Training of Neural Network Approximators

For simplicity, we take the variance of the white noise $g(t) = 1$. Then $G(t) = t(1-t)$.

Forward Training Objective: We design a neural network ϵ_θ to minimize, for $t = 1, \dots, T$, $\epsilon \sim \mathcal{N}(0, I)$,

$$\|X_t - X_0 - \epsilon_\theta(X_t, t)\| = \quad (7)$$

$$\|t(Y - X_0) + \sqrt{t(1-t)}\epsilon - \epsilon_\theta(X_t, t)\|.$$

Here X_t is defined by Equation 3 with $G(t) = t(1-t)$. This is the same training process as that of the Brownian bridges[47]. That is, we do the back propagation of

$$\|t(Y - X_0) + \sqrt{t(1-t)}\epsilon - \epsilon_\theta(X_t, t)\|,$$

where $t \sim \text{Uniform}(1, \dots, T)$ and $\epsilon \sim \mathcal{N}(0, I)$. Essentially, the neural network ϵ_θ is used to estimate X_0 given X_t at the time step t . Note that an optional conditional network design $\epsilon_\theta(X_t, t, Y)$ can also be used, which may improve the stability and efficiency of model training.

Reverse Training Objective: Independently of the forward training, we design a neural network $Z_\phi(X_t, t)$ to minimize, for $t = 1, \dots, T$,

$$\|z - Z_\phi(X_t, t)\|, \quad z \sim \mathcal{N}(0, I), \quad (8)$$

where X_t is defined by $X_t = (1-t)X_0 + tY + \sqrt{t(1-t)}z$. That is, we do the back propagation of

$$\|z - Z_\phi(X_t, t)\|,$$

where $t \sim \text{Uniform}(0, \dots, T-1)$ and $z \sim \mathcal{N}(0, I)$.

3.3. Sampling

We discretize Equation 4 with $g(t) = 1$ to get the iterative generative formula:

$$X_{t-1} = \left(1 - \frac{\Delta t}{t} \right) X_t + \frac{\Delta t}{t} X_0 - [\bar{W}(t) - \bar{W}(t - \Delta t)] \quad (9)$$

We employ the two neural networks in this way: $X_0 \approx X_t - \epsilon_\theta(X_t, t)$, while $\bar{W}(t) - \bar{W}(t - \Delta t)$ must be approximated with the use of the second neural network Z_ϕ .

We make an observation here: $\bar{W}(t) - \bar{W}(t - \Delta t)$ and $\bar{W}(t + \Delta t) - \bar{W}(t)$ are independent, equivalent random variables. Let $g(t) = 1$ in (4) and (5) to get $X_t = (1-t)X_0 + tY + t \int_1^t \frac{d\bar{W}}{s}$. Then we get

$$\bar{W}(t) - \bar{W}(t - \Delta t) = \bar{W}(t + \Delta t) - \bar{W}(t) \approx$$

$$U(X_{t+1}, t+1) - \left(1 + \frac{\Delta t}{t} \right) U(X_t, t) + \frac{\Delta t}{t} (X_0 - Y), \quad (10)$$

where

$$U(X_t, t) = X_t - Y = (1-t)(X_0 - Y) + t \int_1^t \frac{d\bar{W}}{s}. \quad (11)$$

Hence, by plugging the above estimate into Equation 9, we get the final iterative generative formula

$$X_{t-1} = \left(1 - \frac{\Delta t}{t} \right) X_t + \frac{\Delta t}{t} Y - U(X_{t+1}, t+1) \quad (12)$$

$$+ \left(1 + \frac{\Delta t}{t} \right) U(X_t, t).$$

In the formula (12), replace t by $m_t = \frac{t}{T}$ and Δt by $\frac{1}{T}$ if we apply the uniform sampling schedule with T time steps. Also, we estimate X_0 by

$$\hat{X}_0 = X_t - \epsilon_\theta(X_t, t). \quad (13)$$

Then for $t = T - 1, T - 2, \dots, 2$, we get

$$\begin{aligned} X_{t-1} &= \left(1 - \frac{1}{t}\right) X_t + \frac{1}{t} Y - U(X_{t+1}, t+1) \\ &\quad + \left(1 + \frac{1}{t}\right) U(X_t, t). \end{aligned} \quad (14)$$

Algorithm 1 Forward Approximator Training Algorithm

```

1: Input Paired Dataset  $D_{x,y}$ , Forward Network  $\epsilon_\theta$ , Total
   Time Steps  $T$ 
2: repeat
3:    $x, y \sim D_{x,y}$ 
4:    $t \sim \text{Uniform}(1, \dots, T)$ 
5:    $\epsilon \sim \mathcal{N}(0, I)$ 
6:    $x_t = (1 - \frac{t}{T})x_0 + \frac{t}{T}y + B(t)\epsilon$ 
7:    $\nabla_\theta \|x_t - x_0 - \epsilon_\theta(x_t, t)\|$ 
8: until converged
9: end function

```

Algorithm 2 Reverse Approximator Training Algorithm

```

1: Input Paired Dataset  $D_{x,y}$ , Reverse Network  $Z_\phi$ , Total
   Time Steps  $T$ 
2: repeat
3:    $x, y \sim D_{x,y}$ 
4:    $t \sim \text{Uniform}(1, \dots, T)$ 
5:    $z \sim \mathcal{N}(0, I)$ 
6:    $x_t = (1 - \frac{t}{T})x_0 + \frac{t}{T}y + B(t)z$ 
7:    $\nabla_\phi \|z - Z_\phi(x_t, t)\|$ 
8: until converged
9: end function

```

This iterative formula does not apply when $t = T$ as X_{T+1} does not exist. So we define X_{T-1} as we would in the SDE model

$$X_{T-1} = Y - \frac{1}{T}\epsilon_\theta(Y, T) - \frac{1}{\sqrt{T}}z, \quad z \sim \mathcal{N}(0, I). \quad (15)$$

Finally, we define

$$\hat{X}_0 = X_1 - \epsilon_\theta(X_1, 1) \quad (16)$$

as the final output of the algorithm.

The only randomness introduced in the entire sampling process is in X_{T-1} , which should be negligible, as the coefficient $\frac{1}{\sqrt{T}}$ of z is fairly small compared to that of Y . On the contrary, SDE models introduce randomness at every sampling step and hence cause substantial diversity to the output.

3.4. Algorithm

In a given paired dataset $D_{x,y}$, (x, y) denotes a paired images from the set. Define $B(t) = G\left(\frac{t}{T}\right) = \frac{1}{T}\sqrt{t(T-t)}$,

and we have the training and sampling algorithms shown in Algorithms 1 to 3, respectively.

Algorithm 3 Sampling Algorithm (Refactored)

Input: $y, \epsilon_\theta, Z_\phi$

Output: x_0

```

1:  $x_t = y$ 
2: for  $t = T$  to 1 do
3:    $\hat{x}_0 = x_t - \epsilon_\theta(x_t, t)$ 
4:    $\hat{z} \sim \mathcal{N}(0, I)$  if  $t == T$  else  $\hat{z} = Z_\phi(x_t, t)$ 
5:    $\hat{x}_t = (1 - \frac{t}{T})\hat{x}_0 + \frac{t}{T}y + B(t)\hat{z}$ 
6:    $\hat{x}_{t-1} = (1 - \frac{t-1}{T})\hat{x}_0 + \frac{t-1}{T}y + B(t-1)\hat{z}$ 
7:    $U_{t+1} = \hat{x}_t - y, U_t = \hat{x}_{t-1} - y$ 
8:    $x_{t-1} = (1 - \frac{1}{t})x_t + \frac{1}{t-1}y - \frac{1}{t(t-1)}\hat{x}_0 - U_{t+1} + \frac{t}{t-1}U_t$ 
9: end for
10:  $x_0 = \hat{x}_0$ 
11: return  $x_0$ 

```

4. Experiments

In this section, we verify the capability of Dual-approx Bridge, addressing the following questions:

- How do varying the number of sampling steps impact its performance in terms of image quality and faithfulness to GT? Furthermore, how does the sampling variance of our model compare to that of SDE-based samplers in terms of faithfulness to GT?
- How does Dual-approx Bridge perform in terms of faithfulness to GT compared to other models in image-to-image translation tasks that demand high faithfulness and deterministic result?
- How does Dual-approx Bridge perform in general image-to-image translation tasks, which prioritize image quality, when compared to other models including GANs, Diffusion models, and Bridge models?

To address these questions, we used datasets with the following resolutions: Cityscapes [10] (256×256), Edges2Handbags [56] (64×64), DF2K [45] (256×256), Urban100 [22] (256×256 patches), and BSD100 [34] (256×256 patches). For evaluation, we used FID [18] to assess image realism (lower is better), LPIPS [53] for perceptual similarity (lower is better), PSNR for pixel-level similarity (higher is better) and SSIM [49] for structural similarity (closer to 1 is better). Our super-resolution (SR) experiments followed the experimental design of [8]. All of our experiments were implemented using PyTorch [38] and were run on a machine with two NVIDIA RTX A6000 GPUs.

Steps	FID ↓	LPIPS ↓	PSNR ↑	SSIM % ↑
1,000	42.70	0.442	15.10 ± 0.02	$(43.2 \pm 0.07) \%$
200	48.70	0.492	15.70 ± 0.02	$(53.2 \pm 0.06) \%$
10	57.43	0.530	15.62 ± 0.02	$(55.3 \pm 0.06) \%$
3	56.07	0.523	16.99 ± 0.01	(57.4 ± 0.00) \%

Table 1. Quantitative comparison with different sampling steps on the Cityscapes dataset. **Bold** values represent the best performance. Standard Deviation is obtained by five sampling trials for the same input.

4.1. Ablation Study

4.1.1. Impact of Sampling Steps

We first evaluate the impact of sampling steps on our model’s performance in the label-to-photo translation task on the Cityscapes dataset. Since the forward approximator in our model can predict x_0 given x_t , sampling can be stopped at any time, allowing us to test sampling performance with a different number of steps. Table 1 presents how the varying sampling steps affect both image quality and faithfulness. It demonstrates that 1,000 sampling steps yield satisfactory image quality, with FID reaching a minimum of 42.70 and LPIPS dropping to 0.442. However, this comes at the cost of reduced faithfulness when compared to results obtained using fewer sampling steps, as evidenced by the decline in PSNR and SSIM. Notably, with only three sampling steps, our model achieves its peak in terms of faithfulness, attaining 16.99 PSNR and 57.4% SSIM. This demonstrates the model’s adaptability to meet the diverse requirements of various applications.

Additionally, we assessed the variance of the output fidelity in five independent sampling trials given the same input. Clearly, even at a higher sampling step of 1,000, the standard deviation of PSNR and SSIM remained low (0.02 and 0.07%, respectively), and it approaches zero with three sampling steps. This robustness underscores the superiority of our model in consistently producing high-quality and faithful results with minimal variability. Consequently, we employed *three sampling steps* for better robustness and higher efficiency in our subsequent experiments, unless otherwise specified. Our experiments show that three iterations perform well across these metrics, though further research is needed to determine the optimal number of sampling steps for different tasks.

4.1.2. Faithfulness Evaluation

We then compare the faithfulness of Dual-approx Bridge to other Brownian bridge models with SDE-based [27, 47] and PF-ODE-based samplers on the Cityscapes dataset using PSNR and SSIM metrics. Both the SDE-based and PF-ODE-based samplers use 1,000 sampling steps. The Brownian bridge model, as the leading I2I translation method, is an ideal benchmark for us due to the same bridge structure.

As shown in Table 2, our Dual-approx Bridge clearly

Method	PSNR ↑	SSIM % ↑
Brown Bridge Model (SDE)	14.28 ± 0.21	$(49.6 \pm 0.63) \%$
Brown Bridge Model (PF-ODE)	15.23 ± 0.00	$(51.2 \pm 0.00) \%$
Ours	16.99 ± 0.01	$(57.4 \pm 0.00) \%$

Table 2. Quantitative comparison with Brownian bridges using SDE and PF-ODE-based samplers on Cityscape. **Bold** values represent the best performance. Standard deviation is obtained by five sampling trials for the same input.

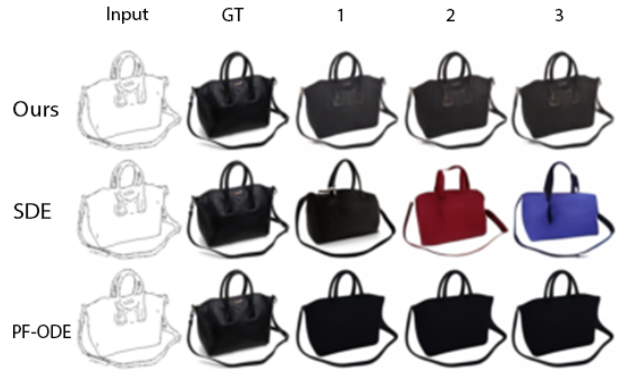


Figure 3. Qualitative comparison with Brownian bridges using SDE-based and PF-ODE-based samplers on Edges2Handbags. Three sampling trials are conducted by each model given the same input. Standard deviation among sampling results by our model, SDE-based and PF-ODE-based sampler are 0.0001, 0.1030 and 0, respectively.

outperforms SDE-based and PF-ODE-based samplers. The PSNR value increased by approximately 12% compared to the second-best, the PF-ODE-based sampler, while the SSIM value showed an overall improvement of 12%, rising from 51.2% to 57.4%. Notably, the metrics of the Dual-approx Bridge exhibited minimal variance, whereas SDE-based sampler exhibited substantial variance in PSNR and SSIM due to the presence of white noise in every step of its sampling.

Figure 3 shows three sample images by each model with the same input in the Edges2Handbags dataset. The images generated by SDE-based sampler are rich in detail but distinct from each other. The PF-ODE-based sampler produces consistent results but lacks details, resulting in a blurred appearance. As a comparison, Dual-approx Bridge achieves SDE-level quality with high and consistent faithfulness.

4.2. Deterministic Image-to-Image Translation

We selected the label-to-photo task in the Cityscapes dataset for deterministic image generation, where the goal is to generate realistic images from segmentation maps. Faithfulness is essential in this task, as it ensures the generated images accurately reflect the structure and content of the input labels, preserving the integrity of labeled features. We also in-

Method	FID ↓	PSNR ↑	SSIM % ↑
Pix2pix	101.04	12.86	28.63 %
CycleGAN	75.37	14.53	34.16 %
UNIT	82.74	14.61	35.41 %
Ours	48.70	15.70	53.26 %

Table 3. Quantitative comparison with deterministic models on Cityscape. Results of our model are obtained using 200 sampling steps. **Bold** values represent the best performance.

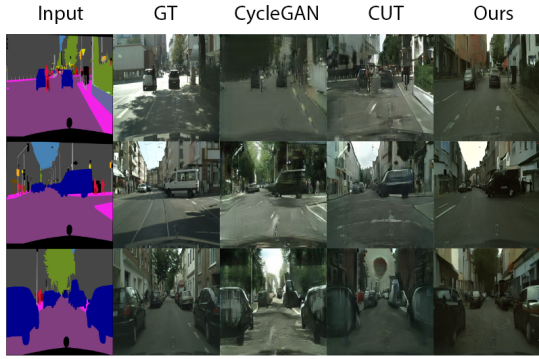


Figure 4. Qualitative comparison between Dual-approx Bridge and SOTA methods on the Cityscapes dataset.



Figure 5. Qualitative comparison on BSD100 datasets.

cluded image super-resolution as a deterministic image-to-image translation task, which also requires both high quality and faithfulness.

Given the inherent randomness in diffusion models, we primarily chose GAN-based models as baselines for deterministic I2I tasks. We selected Pix2Pix [24], CycleGAN [57], and UNIT [31] for comparison on the Cityscapes dataset. For image super-resolution, we used ESRGAN [48], RankSRGAN [52], and SRDiff [28] as baselines and followed the experimental configuration in [33] to train our model on DF2K and test it on Urban100 and BSD100.

Table 3 compares our model against baseline models on the Cityscapes dataset. The Dual-approx Bridge model demonstrates superior performance across all metrics compared to the other models. In terms of image quality, our model achieves a significant improvement in FID, with a score of 48.70 compared to the second-best score of 75.37, representing a substantial 35% performance enhancement. Furthermore, our model exhibits notable gains in PSNR and SSIM, with PSNR increased from 14.61 to 15.70 and SSIM

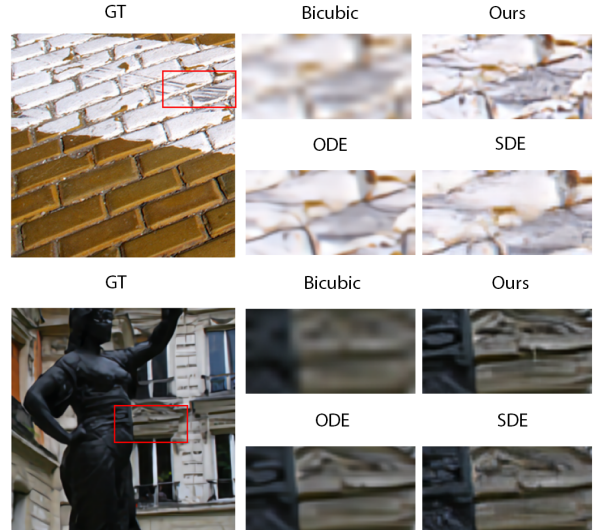


Figure 6. Qualitative comparison on Urban100 datasets.

Model	BSD100		Urban100	
	LPIPS ↓	PSNR ↑	LPIPS ↓	PSNR ↑
Bicubic	0.5282	24.32	0.4826	21.75
ESRGAN	0.1579	23.65	0.1226	23.04
RankSRGAN	0.1714	23.80	0.1403	23.16
SRDiff	0.2046	24.17	0.1391	23.88
Ours	0.1267	26.56	0.1207	23.23

Table 4. Quantitative comparisons on BSD100 and Urban100. **Bold** values represent the best performance.

improved by approximately 50% (from 35.41% to 53.26%). Qualitative comparisons of various methods are presented in Figure 4.

Table 4 compares our model against baselines on super-resolution tasks. Our model performed the best on the BSD100 dataset with LPIPS at 0.1267 and PSNR at 26.56. It also achieves the highest LPIPS score of 0.1207 and the second-highest PSNR score of 23.23 on the Urban100 dataset. While SRDiff achieved the best PSNR on Urban100, its diffusion process encounters challenges in consistently producing stable outputs due to the inherent randomness in its SDE-based sampler (as shown in Table 2). Moreover, our model accomplishes this performance with significantly fewer sampling steps (3 used in our model vs. 1,000 used in SRDiff).

Figure 5 compares the visual quality of various methods for image super-resolution. The top-right of each image shows a zoomed-in view of the red-boxed region for a detailed comparison. Due to inherent randomness, SDEs often introduce unrealistic artifacts, as seen in the example. The PF-ODE-based sampler results exhibit excessive smoothness and the loss of details, as evident in the zoomed



Figure 7. Qualitative comparison between Dual-approx Bridge and SOTA methods on the Edges2handbags dataset.

Method	FID ↓
MUNIT	91.4
DRIT	155.3
Distance	85.8
SelfDistance	78.8
CGGAN	105.2
CUT	56.4
FastCUT	68.8
DCLGAN	49.4
SimDCL	51.3
Ours	48.7

Table 5. Quantitative comparison of image quality on Cityscapes (label to photo). **Bold** values represent the best performance.



Figure 8. Quantitative comparison between Dual-approx Bridge and A-bridge (with SDE-based sampler). Each model are sampled five times given the same input. Sampling standard deviation of the first example (Ours: 0.0084, A-bridge: 0.0903) and the second example (Ours: 0.0054, SDE: 0.0672).

regions for both examples. Figure 6 further illustrates that our model can achieve detail preservation approaching or even surpassing that of SDE-based methods. Conversely, the Dual-approx Bridge method demonstrates a remarkable ability to preserve details while maintaining high faithfulness with GT.

4.3. General Image-to-Image Translation

Finally, we evaluate Dual-approx Bridge on general image-to-image translation tasks. We assess our model’s image quality on the Edges2Handbags and Cityscapes datasets. For Edges2Handbags, we conduct comparisons with Pix2Pix [24], SDEdit [35], DDIB [44], Rectified Flow [32], I2SB [30], DDBM [54], and A-bridge [47]. For the

Method	FID ↓
Pix2Pix	74.8
DDIB	186.84
SDEdit	85.8
SelfDistance	26.5
Rectified Flow	25.3
I2SB	7.43
DDBM (VP)	1.83
A-Bridge	1.07
Ours	1.36

Table 6. Quantitative comparison of image quality on Edges2Handbags. **Bold** values represent the best performance.

Cityscapes dataset, we compared our model with MUNIT [23], DRIT [26], DistanceGAN [3], Self-DistanceGAN [3], CGGAN [55], CUT [37], FastCUT [37], DCLGAN [17], and SimDCL [17].

On the Cityscapes dataset, our model outperforms all GAN-based models, achieving the top position and surpassing all competitors (Table 5). As shown in Table 6, our model achieves 1.36 FID score on the Edges2Handbags dataset, securing the second place. This result demonstrates that, despite our primary focus on enhancing faithfulness, our model still delivers highly competitive image quality.

Figure 7 provides a qualitative comparison of our model with A-bridge on the Edges2Handbags dataset. Although A-bridge achieves the best FID score, it uses SDE-based samplers. As shown in Figure 8, our model demonstrates much higher faithfulness and consistency across repeated sampling with far fewer sampling steps (3 in our model vs. 50 in A-bridge).

5. Conclusion and Future Work

In this paper, we proposed Dual-approx Bridge, a novel generative model to produce faithful and high quality output for deterministic I2I translations. Our extensive experiments on benchmark datasets demonstrate the consistent and superior performance of Dual-approx Bridge when compared to SOTA I2I models. Our current choice of the SDE follows the Variance Preserving (VP) formulation. Moving forward, we plan to explore the potentials of combining both VP and variance exploding SDEs to further enhance our model’s capabilities.

References

- [1] Aziz Alotaibi. Deep generative adversarial networks for image-to-image translation: A review. *Symmetry*, 12(10), 2020. [1](#) [2](#)
- [2] Brian D.O. Anderson. Reverse-time diffusion equation models. *Stochastic Processes and their Applications*, 12(3):313–326, 1982. [4](#)
- [3] Sagie Benaim and Lior Wolf. One-sided unsupervised domain mapping. *Advances in neural information processing systems*, 30, 2017. [8](#)
- [4] Marcelo Bertalmio, Guillermo Sapiro, Vicent Caselles, and Coloma Ballester. Image inpainting. *Proceedings of the 27th annual conference on Computer graphics and interactive techniques*, 2000. [1](#)
- [5] Ali Borji. Pros and cons of gan evaluation measures. *Computer vision and image understanding*, 179:41–65, 2019. [2](#) [3](#)
- [6] Antoni Buades, Bartomeu Coll, and Jean-Michel Morel. A non-local algorithm for image denoising. *Computer Vision and Pattern Recognition*, 2005. [1](#)
- [7] Yun Cao, Zhiming Zhou, Weinan Zhang, and Yong Yu. Unsupervised diverse colorization via generative adversarial networks. In *Machine Learning and Knowledge Discovery in Databases: European Conference, ECML PKDD 2017, Skopje, Macedonia, September 18–22, 2017, Proceedings, Part I 10*, pages 151–166. Springer, 2017. [2](#)
- [8] Yue Chen, Mingwei Sun, and Chao Dong. Solving diffusion ODEs with optimal boundary conditions for better image super-resolution. *arXiv preprint arXiv:2302.10041*, 2023. [1](#) [5](#)
- [9] Zhentao Cheng, Qingxiong Yang, and Bin Sheng. Deep colorization. In *Proceedings of the IEEE international conference on computer vision*, 2015. [2](#)
- [10] Marius Cordts, Mohamed Omran, Sebastian Ramos, Timo Rehfeld, Markus Enzweiler, Rodrigo Benenson, Uwe Franke, Stefan Roth, and Bernt Schiele. The cityscapes dataset for semantic urban scene understanding. In *Proceedings of the IEEE conference on computer vision and pattern recognition*, pages 3213–3223, 2016. [5](#)
- [11] Prafulla Dhariwal and Alexander Nichol. Diffusion models beat gans on image synthesis. *Advances in neural information processing systems*, 34:8780–8794, 2021. [3](#)
- [12] Chao Dong, Chen Change Loy, Kaiming He, and Xiaouo Tang. Image super-resolution using deep convolutional networks. *IEEE Transactions on Pattern Analysis and Machine Intelligence*, 38(2):295–307, 2016. [2](#)
- [13] Tsao Li-Yuan et al. Boosting flow-based generative SR models via learned prior. In *CVPR*, pages 26005–26015, 2024. [1](#)
- [14] Wu Hongjie et al. Diffusion posterior proximal sampling for image restoration. In *ACM MM*, pages 214–223, 2024. [1](#)
- [15] Leon A Gatys, Alexander S Ecker, and Matthias Bethge. A neural algorithm of artistic style. *arXiv preprint arXiv:1508.06576*, 2015. [2](#)
- [16] Ian J. Goodfellow, Jean Pouget-Abadie, Mehdi Mirza, Bing Xu, David Warde-Farley, Sherjil Ozair, Aaron Courville, and Yoshua Bengio. Generative adversarial nets. In *Proceedings of the Advances in Neural Information Processing Systems (NeurIPS)*, pages 2672–2680, 2014. [1](#) [2](#)
- [17] Junlin Han, Mehrdad Shoeiby, Lars Petersson, and Mohammad Ali Armin. Dual contrastive learning for unsupervised image-to-image translation. In *Proceedings of the IEEE/CVF conference on computer vision and pattern recognition*, pages 746–755, 2021. [8](#)
- [18] Martin Heusel, Hubert Ramsauer, Thomas Unterthiner, Bernhard Nessler, and Sepp Hochreiter. Gans trained by a two time-scale update rule converge to a local nash equilibrium. In *Advances in neural information processing systems*, pages 6626–6637, 2017. [5](#)
- [19] Jonathan Ho, Ajay Jain, and Pieter Abbeel. Denoising diffusion probabilistic models. In *Advances in Neural Information Processing Systems (NeurIPS)*, pages 6840–6851, 2020. [1](#)
- [20] Jonathan Ho, Ajay Jain, and Pieter Abbeel. Denoising diffusion probabilistic models. In *Advances in Neural Information Processing Systems (NeurIPS)*, pages 6840–6851, 2020. [3](#)
- [21] Henri Hoyez, Cédric Schockaert, Jason Rambach, Bruno Mirbach, and Didier Stricker. Unsupervised image-to-image translation: A review. *Sensors*, 22(21), 2022. [1](#) [2](#)
- [22] Jia-Bin Huang, Abhishek Singh, and Narendra Ahuja. Single image super-resolution from transformed self-exemplars. In *Proceedings of the IEEE conference on computer vision and pattern recognition*, pages 5197–5206, 2015. [5](#)
- [23] Xun Huang, Ming-Yu Liu, Serge Belongie, and Jan Kautz. Multimodal unsupervised image-to-image translation. In *ECCV*, pages 172–189, 2018. [8](#)
- [24] Phillip Isola, Jun-Yan Zhu, Tinghui Zhou, and Alexei A. Efros. Image-to-image translation with conditional adversarial networks. In *CVPR*, pages 1125–1134, 2017. [1](#) [2](#) [7](#) [8](#)
- [25] Beomsu Kim, Gihyun Kwon, Kwanyoung Kim, and Jong Chul Ye. Unpaired image-to-image translation via neural schr\” odinger bridge. *arXiv preprint arXiv:2305.15086*, 2023. [3](#)
- [26] Hsin-Ying Lee, Hung-Yu Tseng, Jia-Bin Huang, Maneesh Singh, and Ming-Hsuan Yang. Diverse image-to-image translation via disentangled representations. In *ECCV*, pages 35–51, 2018. [8](#)
- [27] Bo Li, Kaitao Xue, Bin Liu, and Yu-Kun Lai. Bbdm: Image-to-image translation with brownian bridge diffusion models. In *Proceedings of the IEEE/CVF conference on computer vision and pattern Recognition*, pages 1952–1961, 2023. [1](#) [2](#) [3](#) [6](#)
- [28] Zhengxiong Li, Qiaosi Yi, Deng-Ping Fan, Jufeng Yang, Ali Borji, Ling Shao, and Luc Van Gool. Srdiff: Single image super-resolution with diffusion probabilistic models. *IEEE Transactions on Pattern Analysis and Machine Intelligence*, 2022. [1](#) [7](#)
- [29] Geert Litjens, Thijs Kooi, Babak Ehteshami Bejnordi, et al. A survey on deep learning in medical image analysis. *Medical Image Analysis*, 42:60–88, 2017. [2](#)
- [30] Guan-Horng Liu, Arash Vahdat, De-An Huang, Evangelos A Theodorou, Weili Nie, and Anima Anandkumar.

I2sb: Image-to-image schrodinger bridge. *arXiv preprint arXiv:2302.05872*, 2023. 3, 8

[31] Ming-Yu Liu, Thomas Breuel, and Jan Kautz. Unsupervised image-to-image translation networks. *Advances in neural information processing systems*, 30, 2017. 7

[32] Xingchao Liu, Chengyue Gong, and Qiang Liu. Flow straight and fast: Learning to generate and transfer data with rectified flow. *arXiv preprint arXiv:2209.03003*, 2022. 8

[33] Yiyang Ma, Huan Yang, Wenhan Yang, Jianlong Fu, and Jiaying Liu. Solving diffusion odes with optimal boundary conditions for better image super-resolution. *arXiv preprint arXiv:2305.15357*, 2023. 7

[34] David Martin, Charless Fowlkes, Doron Tal, and Jitendra Malik. A database of human segmented natural images and its application to evaluating segmentation algorithms and measuring ecological statistics. *Proceedings Eighth IEEE International Conference on Computer Vision. ICCV 2001*, 2:416–423, 2001. 5

[35] Chenlin Meng, Yutong He, Yang Song, Jiaming Song, Jianjun Wu, Jun-Yan Zhu, and Stefano Ermon. Sdedit: Guided image synthesis and editing with stochastic differential equations. *arXiv preprint arXiv:2108.01073*, 2021. 8

[36] Yingxue Pang, Jianxin Lin, Tao Qin, and Zhibo Chen. Image-to-image translation: Methods and applications. *IEEE Transactions on Multimedia*, 24:3859–3881, 2021. 2

[37] Taesung Park, Alexei A Efros, Richard Zhang, and Jun-Yan Zhu. Contrastive learning for unpaired image-to-image translation. In *Computer Vision–ECCV 2020: 16th European Conference, Glasgow, UK, August 23–28, 2020, Proceedings, Part IX 16*, pages 319–345. Springer, 2020. 8

[38] Adam Paszke et al. Pytorch: An imperative style, high-performance deep learning library. In *NIPS*, pages 8024–8035. Curran Associates, Inc., 2019. 5

[39] Deepak Pathak, Philipp Krahenbuhl, Jeff Donahue, Trevor Darrell, and Alexei A Efros. Context encoders: Feature learning by inpainting. In *Proceedings of the IEEE conference on computer vision and pattern recognition*, 2016. 1

[40] Robin Rombach, Andreas Blattmann, Dominik Lorenz, Patrick Esser, and Björn Ommer. High-resolution image synthesis with latent diffusion models. In *CVPR*, pages 10684–10695, 2022. 1, 3

[41] Konstantin Shmelkov, Cordelia Schmid, and Karteek Alahari. How good is my gan? In *ECCV*, pages 213–229, 2018. 2, 3

[42] Yang Song and Stefano Ermon. Generative modeling by estimating gradients of the data distribution. *Advances in neural information processing systems*, 32, 2019. 1

[43] Yang Song, Jascha Sohl-Dickstein, Diederik P Kingma, Abhishek Kumar, Stefano Ermon, and Ben Poole. Score-based generative modeling through stochastic differential equations. *arXiv preprint arXiv:2011.13456*, 2020. 1, 3

[44] Xuan Su, Jiaming Song, Chenlin Meng, and Stefano Ermon. Dual diffusion implicit bridges for image-to-image translation. *arXiv preprint arXiv:2203.08382*, 2022. 8

[45] Radu Timofte, Eirikur Agustsson, Luc Van Gool, Ming-Hsuan Yang, Lei Zhang, Bee Lim, Sanghyun Son, Heewon Kim, Seungjun Nah, Kyoung Mu Lee, et al. Ntire 2017 challenge on single image super-resolution: Methods and results. In *Proceedings of the IEEE conference on computer vision and pattern recognition workshops*, pages 114–125, 2017. 5

[46] Dmitry Ulyanov, Andrea Vedaldi, and Victor Lempitsky. Deep image prior. In *CVPR*, pages 9446–9454, 2018. 2

[47] Peiyong Wang, Bohan Xiao, Qisheng He, Carri Glide-Hurst, and Ming Dong. Score-based image-to-image brownian bridge. In *Proceedings of the 32nd ACM International Conference on Multimedia*, page 10765–10773, New York, NY, USA, 2024. Association for Computing Machinery. 1, 2, 3, 4, 6, 8

[48] Xintao Wang, Ke Yu, Shixiang Wu, Jinjin Gu, Yihao Liu, Chao Dong, Chen Change Loy, Yu Qiao, and Xiaou Tang. Esgan: Enhanced super-resolution generative adversarial networks. In *ECCV Workshops*, 2018. 7

[49] Zhou Wang, Alan C Bovik, Hamid R Sheikh, and Eero P Simoncelli. Image quality assessment: from error visibility to structural similarity. *IEEE transactions on image processing*, 13(4):600–612, 2004. 5

[50] Zhou Wang, Quan She, and Tomas E. Ward. Generative adversarial networks in computer vision: A survey and taxonomy. *ACM Computing Surveys (CSUR)*, 54(2):1–38, 2021. 3

[51] Kai Zhang, Wangmeng Zuo, Yunjin Chen, Dongwei Meng, and Lei Zhang. Beyond a gaussian denoiser: Residual learning of deep cnn for image denoising. In *IEEE Transactions on Image Processing*, 2017. 1

[52] Kai Zhang, Luc Van Gool, and Radu Timofte. Ranksrgan: Generative adversarial networks with ranker for image super-resolution. *IEEE Transactions on Pattern Analysis and Machine Intelligence*, 43(6):2158–2174, 2021. 1, 7

[53] Richard Zhang, Phillip Isola, Alexei A Efros, Eli Shechtman, and Oliver Wang. The unreasonable effectiveness of deep features as a perceptual metric. *Proceedings of the IEEE Conference on Computer Vision and Pattern Recognition*, pages 586–595, 2018. 5

[54] Linqi Zhou, Aaron Lou, Samar Khanna, and Stefano Ermon. Denoising diffusion bridge models. *arXiv preprint arXiv:2309.16948*, 2023. 1, 3, 8

[55] Zhaorun Zhou and Zhenghao Shi. Cggan: a context-guided generative adversarial network for single image dehazing. *IET Image Processing*, 14(15):3982–3988, 2020. 8

[56] Jun-Yan Zhu, Philipp Krähenbühl, Eli Shechtman, and Alexei A Efros. Generative visual manipulation on the natural image manifold. In *ECCV*, pages 597–613. Springer, 2016. 5

[57] Jun-Yan Zhu, Taesung Park, Phillip Isola, and Alexei A. Efros. Unpaired image-to-image translation using cycle-consistent adversarial networks. In *ICCV*, pages 2223–2232, 2017. 1, 2, 7